Electrical Supporting Information (ESI) for

Improvement on Piezoresistive Sensing Behavior of Graphene Sponge by Polyaniline Nanoarrays

Jingxia Huang [ab], Honggang Wang [a], Zhangpeng Li [a]*, Xianzhang Wu [ab], Jinqing Wang [a]*, and Shengrong Yang [ab]

[a] State Key Laboratory of Solid Lubrication, Lanzhou Institute of Chemical Physics, Chinese Academy of Sciences, Lanzhou 730000, China.

[b] Center of Materials Science and Optoelectronics Engineering, University of Chinese Academy of Sciences, Beijing 100049, China

* Corresponding authors.

Tel: +86-931-4968076; Fax: +86-931-4968019.

E-mail address: jqwang@licp.cas.cn (J. Q. Wang); zhangpengli@licp.cas.cn (Z. P. Li)

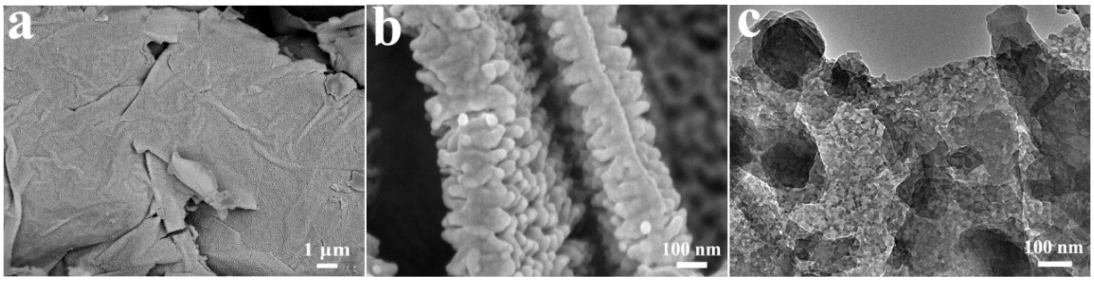

Fig. S1. (a-b) SEM morphologies of GO@PANI showed PANI nanowires uniformly grow on the side of GO nanosheets without obvious aggregation, and (c) the corresponded TEM image presented an interactive nanostructure combining of the rGO sheet and PANI arrays.

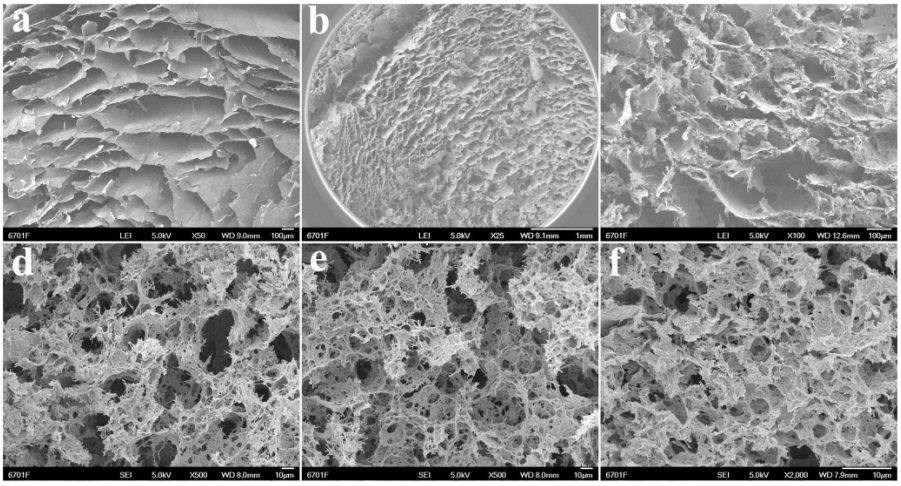

Fig. S2 SEM morphologies of rGPS-x composites: (a) rGPS-0.5, (b) rGPS-1, (c) rGPS-2, (d) rGPS-3, (e) rGPS-5, (f) rGPS-7, respectively.

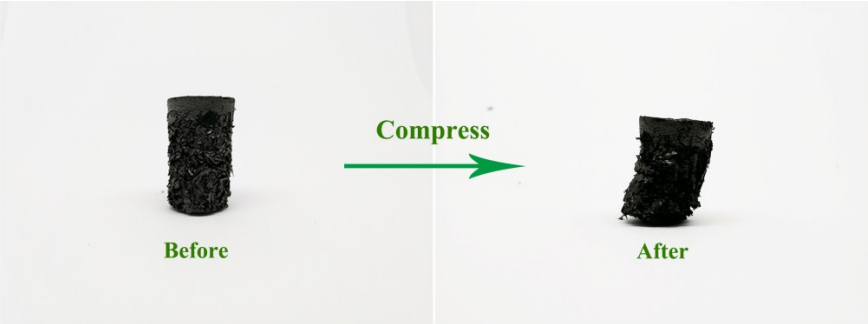

Fig. S3 Optical images of rGPS-3 composite during the compression.

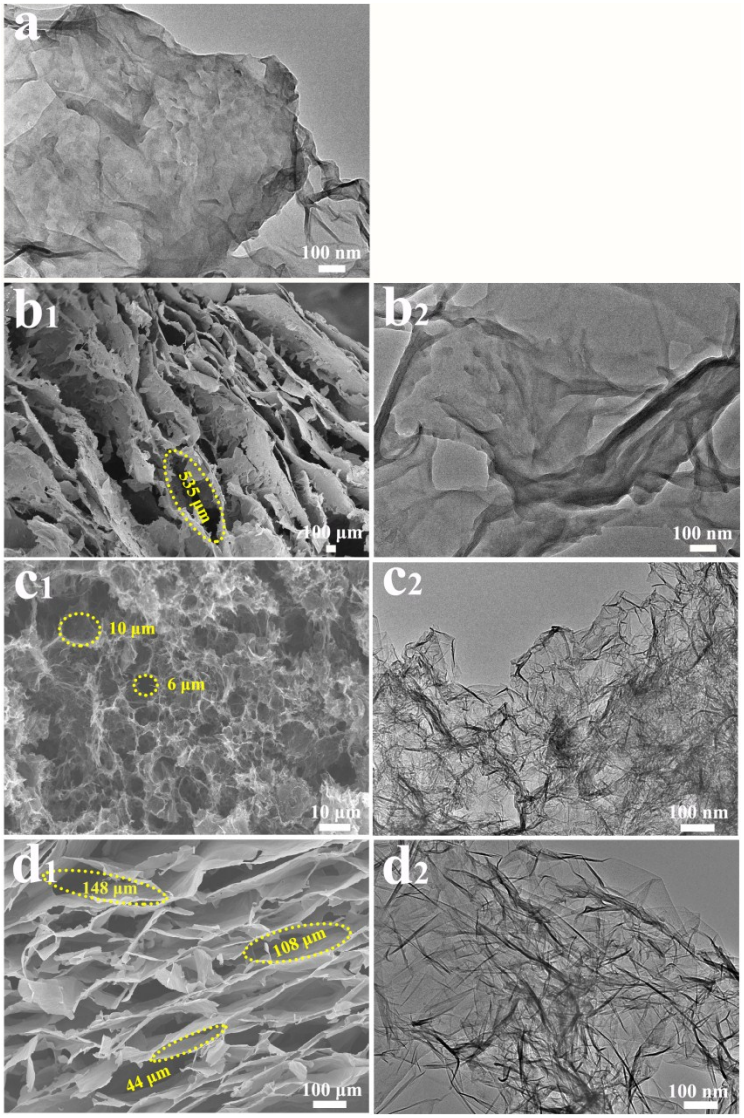

Fig. S4 (a) TEM image of rGPS composite presented the interactive nanostructure between rGO and GO@PANI sheets. (b_1-b_2) SEM image of GPS composite presented the large and thick lamellar structure as well as TEM image showed the opaque sheet.

(c_1-c_2) SEM image of GS presented the disordered microstructure and TEM image of GS showed the typical wrinkles. (d_1-d_2) SEM image of rGS presented the ordered network nanostructure and TEM image showed the clear and mild wrinkles, respectively.

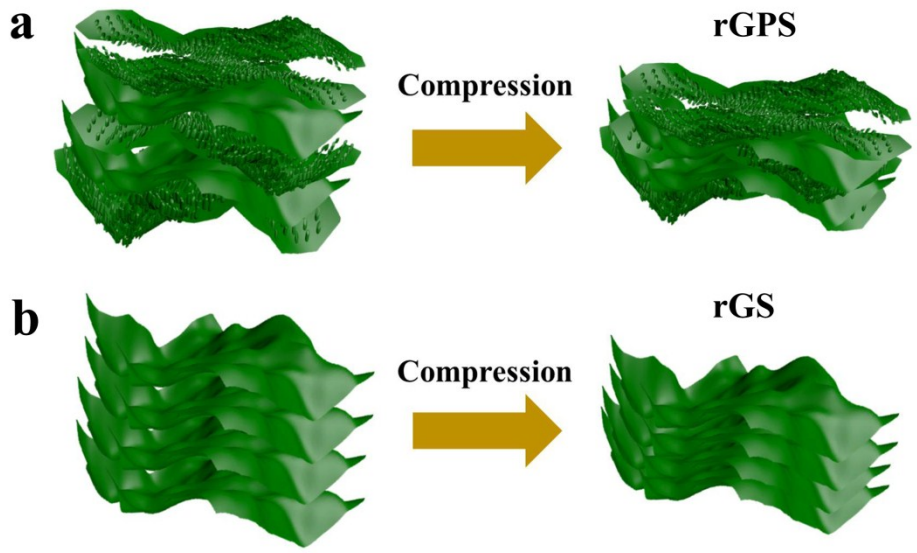

Fig. S5 Schematic diagrams of rGPS composite material-based sensor (a) and rGS material-based sensor (b).

As shown in Fig. S6, the sensitivity of rGPS-*x*-based sensors is increasing with GO concentration decreases within limits or the mass ratio (*x*) of GO@PANI to GO increases. Here the sensor based on rGPS-0.5 composite possesses 0.34 kPa^{-1} of the sensitivity, as the mass ratio of GO@PANI to GO increases to 3, the sensitivity of the sensor based on rGPS-3 composite also rises to 1.10 kPa^{-1} of the value. The increased sensitivity is caused by the rising numbers of the contact pairs between two layer interfaces in rGPS-*x* composite with the abundant PANI nanoarrays and multilevel porous architecture due to the mass ratio of GO@PANI to GO increases. Notably, as the mass ratio (*x*) of GO@PANI to GO over 3, the mechanical properties of the as-

prepared rGPS-*x* composite become worse due to the serious collapse of the network structure after compression, and thus the measurement of sensitivity is meaningless. In our experiment, rGPS-1 composite obtained from the mass ratio (*x*=1) of GO@PANI to GO exhibits the high sensitivity of 0.77 kPa^{-1} due to the decent mechanical property and the relative ordered network architecture as well as the apparent PANI nanoarrays decorated onto rGO porous architecture.

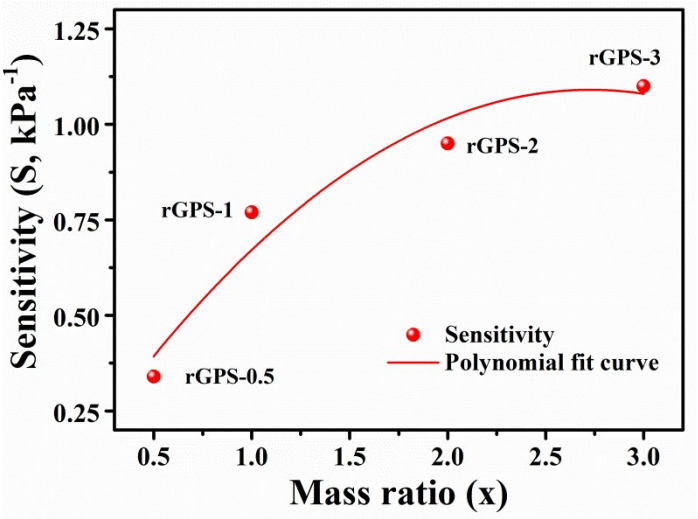

Fig. S6 The relationship between the mass ratio (*x*) of GO@PANI to GO and the sensitivity of the sensors based on rGPS-*x* composites.

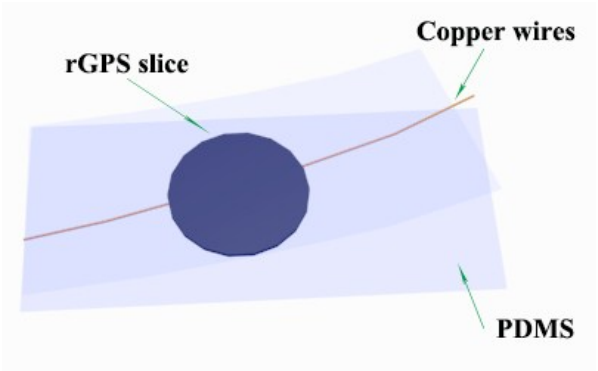

Fig. S7 Structure diagram of the sensor device based on rGPS composite.

Table S1 The elemental composition of XPS analysis for GS, GO@PANI, GPS, and rGPS composite.

Samples	C (at. %)	N (at. %)	O (at. %)	Cl (at. %)
GS	83.83	--	16.17	--
GO@PANI	78.12	6.96	11.42	3.51
GPS	83.63	5.83	10.04	0.50
rGPS	83.30	10.29	6.28	0.22

Table S2 The relative ratio of different carbon chemical bonds in the GO@PANI, GPS, and rGPS composite.

Samples	-N=	Pyridinic N	-NH-	N^+
GO@PANI	9.35	--	54.61	36.04
GPS	18.69	--	47.23	34.08
rGPS	18.85	27.15	32.75	21.25

Table S3 Several sensing parameters of the pressure sensor compared with some reported pressure sensors.

Sensing materials	Electrical conductivity ($S\ m^{-1}$)	Maximum sensitivity (kPa^{-1})	Pressure range (kPa)	Maximum stress (kPa)	Response time (ms)	Cycling stability (cycles)	Reference
rGPS	3.54	0.77	0.0364 -29.17	29.17	50	3000	Present work
GO-KGM foam	1.17	0.25	0.015-4	4	40	3000	1
GO-PU sponge	--	0.26	0.009-2	2	--	10000	2
G-ACHF foam	--	~0.0115	0-0.018	0.018	--	200	3
MPS-GA aerogel	1.28	0.22	0-8	8	--	100	4
MX/ rGO aerogel	--	22.56	0.01-4.9	4.9	200	10000	5

rGO-PI foam	~2.2 $\times 10^{-2}$	0.18	0-6.5	6.5	--	2000	6
N-doped 3DG	--	0.045	0.015-10	10	700	--	7
Gr/PDMS arrays	--	8.5	0.001-12	12	40	10000	8
GCNT aerogel	2.4	1.22	0-7	7	28	3000	9
graphene foam	--	1.16	0-9	9	150	10^5	10

References

1 X. Z. Wu, K. M. Hou, J. X. Huang, J. Q. Wang, S. R. Yang, *J. Mater. Chem. C*, 2018, **6**, 8717-8725.

2 H. B. Yao, J. Ge, C. F. Wang, X. Wang, W. Hu, Z. J. Zheng, Y. Ni, S. H. Yu, *Adv. Mater.*, 2013, **25**, 6692-6698.

3 Y. X. Ma, M. Yu, J. H. Liu, X. J. Li, S. M. Li, *ACS Appl. Mater. Interfaces*, 2017, **9**, 27127-27134.

4 P. P. Zhang, L. X. Lv, Z. H. Cheng, Y. Liang, Q. H. Zhou, Y. Zhao, L. T. Qu, *Chem Asian J*, 2016, **11**, 1071-1075.

5 Y. N. Ma, Y. Yue, H. Zhang, F. Cheng, W. Q. Zhao, J. Y. Rao, S. J. Luo, J. Wang, X. L. Jiang, Z. T. Liu, N. S. Liu, Y. H. Gao, *ACS Nano*, 2018, **12**, 3209-3216.

6 Y. Y. Qin, Q. Y. Peng, Y. J. Ding, Z. S. Lin, C. H. Wang, Y. Li, X. Fan, J. J. Li, Y. Yuan, X. D. He, Y. B. Li, *ACS Nano*, 2015, **9**, 8933-8941.

7 M. A. S. M. Haniff, S. M. Hafiz, N. M. Huang, S. A. Rahman, K. A. A. Wahid, M. I. Syono, I. A. Azid, *ACS Appl. Mater. Interfaces*, 2017**, 9**, 15192-15201.

8 G. Y. Bae S. W. Pak, D. Kim, G. Lee, D. H. Kim, Y. Chung, K. Cho, *Adv. Mater.*,

2016, **28**, 5300-5306.

9 X. Z. Wu, X. H. Liu, J. Q. Wang, J. X. Huang, S. R. Yang, *ACS Appl. Mater. Interfaces*, 2018, **10**, 39009-39017.

10 Y. Zhong, X. H. Tan, T. L. Shi, Y. Y. Huang, S. Y. Cheng, C. Chen, G. L. Liao, Z. R. Tang, *Sensor and Actuat. A: Phys.*, 2018, **281**, 141-149.